Learning Good Features for Active Shape Models

Nuria Brunet   Francisco Perez   Fernando De la Torre
Robotics Institute, Carnegie Mellon University, Pittsburgh, Pennsylvania 15213.

Abstract

Active Shape Models (ASMs) are commonly used to model the appearance and shape variation of objects in images. This paper proposes two strategies to improve speed and accuracy in ASMs fitting. First, we define a new criterion to select landmarks that have good generalization properties. Second, for each landmark we learn a subspace with improved facial feature response effectively avoiding local minima in the ASM fitting. Experimental results show the effectiveness and robustness of the approach.

1. Introduction

Active Shape Models (ASMs) [3, 2] have proven to be a powerful tool to model the shape and appearance of faces in images. There are two key components in ASMs: the learning component, that uses Principal Component Analysis (PCA), and the fitting process, typically done with some greedy search [2]. Although widely used, two undesirable effects might occur when using PCA to learn a generic model of an object's appearance. First, the location of the parameters (e.g. translation) fails to correspond to the location of the object (e.g. face). Second, many local minima may be found. Even if a gradient descent algorithm is initialized close to the correct solution, the occurrence of local minima is likely to divert convergence from the desired solution. For instance, consider fig. (1.a), where a face has been labeled with 68 landmarks. For each landmark, a PCA model that preserves 80% of the energy is computed from 600 training images. Figure (1.b) shows the surface of the reconstruction error (distance from the subspace) for different translations (32×32 pixels) around the position of the landmark (black dot). The region of this particular landmark is a good feature because its response has only one local minimum in the expected location. On the other hand, there are regions that are not well suited for detecting facial features in new images. For instance, consider fig. (1.c) that shows the error surface of a landmark in the outline of the face. The error surface has multiple local minima and none in the position of the labeled landmark. In this paper, we propose a method to learn a subspace that improves the surface response, see fig. (1.d). That is, the new error surface has fewer local minima and it has the global minimum on the labeled place. The two main contributions of the paper are: (1) describe a new criterion to select good regions that generalize well for ASMs. (2) learn a subspace that explicitly reduces the number of local minima.

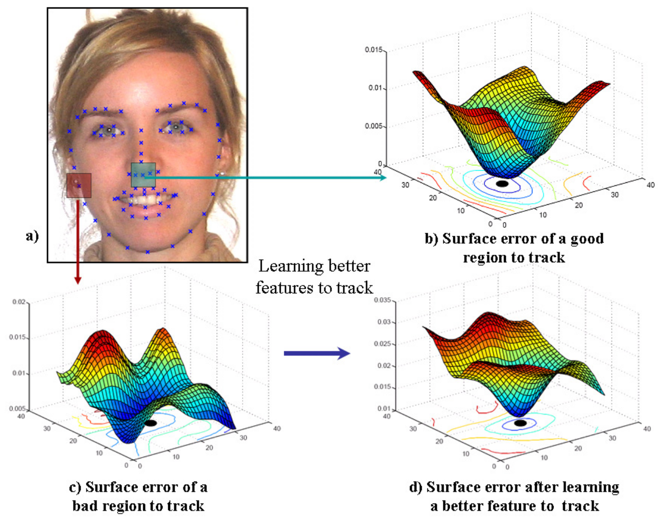

Figure 1. a) Face image labeled with 68 landmarks. b) Reconstruction error (i.e. distance from the subspace) in a 32×32 pixels area around a landmark in the lower part of the nose. The black dot denotes the hand labeled position of the landmark. c) Reconstruction error around an outline landmark. d) Reconstruction error around the same landmark as subplot c after learning better features.

The rest of the paper is organized as follows. Section 2 reviews previous work on ASMs. Section 3 proposes a new criterion to select good regions to track. Section 4 describes a method to learn a subspace that provides good error surfaces to fit ASMs. Section 5 presents experimental results.

2. Previous work

ASMs [2] build a model of shape variation by performing PCA on a set of landmarks (after Procrustes analysis). For each landmark the Mahalanobis distance between the sample and mean texture is used to assess the quality of

2009 IEEE 12th International Conference on Computer Vision Workshops, ICCV Workshops
978-1-4244-4441-0/09/$25.00

fitting to a new shape. The fitting process is performed using a local search along the normal of the landmark. Later, the new positions are projected onto the non-rigid appearance basis and rigid transformations. These two steps are alternated until convergence. Recently, Cristinacce and Cootes [4] introduced extended ASMs with Constrained Local Models that compute local responses with the learned templates of the appearance model. CLM has proven to be a more robust fitting procedure than ASM and AAM.

Although ASMs are widely used, they suffer from large sensitivity to local minima. Several strategies and methods to improve fitting have been proposed: Using multiresolution schemes [2] or Multiband filters [5, 1] have been proposed to improve fitting and generalization in Active Appearance Models (AAMs). Wimmer et al. [10] propose a method to learn one dimensional convex error functions as combinations of Haar-like features. De la Torre and Nguyen [8] learned a weighted subspace for AAMs that explicitly avoids local minima in its fitting. Recently, Wu et al. [11] proposed avoiding local minima in discriminative fitting of appearance models by learning boosting with ranked functions. Although these methods show significant performance improvement, they do not provide a selection mechanism for regions that generalize well. Moreover, methods such as [8, 11] can not guarantee avoiding local minima in all the search space because they only impose constrains in some sampled points. Our method differs from previous literature in two aspects: (1) define a new criterion to select good regions that generalize well for ASMs, (2) propose a 2D supervised PCA method that learns a good error surface to fit ASMs.

3. Selecting good regions for fitting ASMs

Shi and Tomasi [9] present a method to select good features to track. The features (pixels) are selected based on the spatial and temporal statistics of the initial frame and current frame. Similarly in spirit, in this section, we propose a method to select good regions for ASMs based on local minima properties of the surface error.

Given a basis for an appearance model $\mathbf{B} \in \Re^{d \times k}$ (e.g. PCA), and a region in an image $\mathbf{d}_i$ (see notation [1]) (e.g. 32×32 pixels), the optimal placement of the landmark (x, y) in the ASM search is obtained by minimizing:

$$\min_{(a_1,a_2)} \frac{||\mathbf{d}_i^{(x+a_1,y+a_2)} - \boldsymbol{\mu} - \mathbf{B}\mathbf{c}_i||_2^2}{||\mathbf{d}_i^{(x+a_1,y+a_2)}||_2^2} \quad (1)$$

where (a_1, a_2) are the translational parameters and $\mathbf{c}_i$ the appearance coefficients. $\mathbf{d}_i^{(x+a_1,y+a_2)}$ denotes a region around the $(x+a_1, y+a_2)$ position. Searching over the coefficients $\mathbf{c}_i$ and the translations (a_1, a_2) that minimize eq. (1) generates a local error surface (e.g. fig. (1.c)). The number and position of local minima on the surface depend on many factors, such as: how well PCA generalizes, robustness to undesirable noise, number of bases, or the chosen representation (e.g. graylevel, gradients). Not all regions contribute equally to the performance of the ASM. In order to select good regions to track, it is necessary to define a criterion based on local minima properties of the error surface.

To quantitatively compare the regions' responses, we compute three error surface statistics with different patch sizes and PCA energies:

- Number of minima. The amount of local minima on the error surface is calculated by counting the number of points with a sign change in the x and y derivatives and positive second derivative.
- Distance between the global minimum and the expected position of the landmark.
- Distance between the global and closest minimum.

To compute these statistics a local PCA model for each of the 68 landmarks is built, see fig. (2.a). The landmarks have been manually labeled in 600 frontal face images (neutral expression) from the CMU Multi-pie database [7], after Procrustes analysis [2]. The local PCA model is computed for different patch sizes, 20×20, 30×30 and 60×60 pixels, and for three different energies: 60%, 70% and 80%.

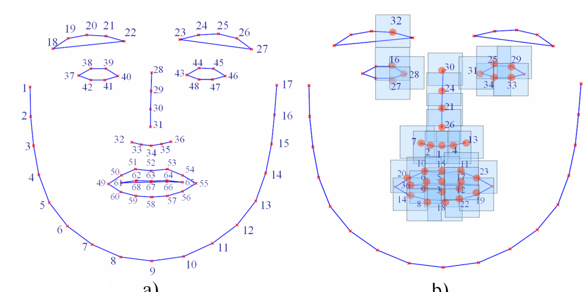

Figure 2. a) 68 landmarks. b) Best 34 patches to track according to eq. 2. The number indicates order of the best regions.

A good region for ASMs is considered if the global minimum is close to the expected location of the landmark. Fig. (3) shows the mean and std of the distance for each of the 68 landmarks. These statistics are computed in 320 testing images (not in the training). As expected, the distance between the global minimum to the desired position is inversely proportional to the energy level. That is, the distance decreases if energy increases. On the other hand, the higher the PCA energy the more likely it is to have more local minima in the patch, see fig. (4). Hence, there is an energy trade-off

[1] Bold capital letters denote a matrix $\mathbf{D}$, bold lower-case letters a column vector $\mathbf{d}$. $\mathbf{d}_j$ represents the j column of the matrix $\mathbf{D}$. d_{ij} denotes the scalar in the row i and column j of the matrix $\mathbf{D}$ and the scalar i-th element of a column vector $\mathbf{d}_j$. All non-bold letters will represent variables of scalar nature. $||\mathbf{x}||_2 = \sqrt{\mathbf{x}^T\mathbf{x}}$ designates Euclidean norm of $\mathbf{x}$.

between having a good localization and the density of local minima.

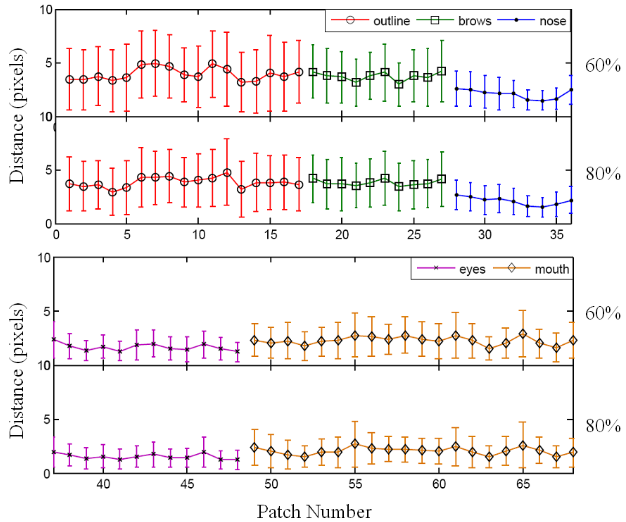

Figure 3. Mean and standard deviation of the distance from the global minimum to the expected position of the landmark. Also the standard deviation is plotted. The statistics are computed for two PCA energies, 60% and 80%. Patch number corresponds to the numbers in fig.(2.a).

The number of local minima also depends on the size of the patch (20×20, 30×30 and 60×60), see fig. (5). Moreover, the density of local minima decreases with the size of the patch. However, the computational complexity of the algorithm scales quadratically with the dimensions of the patch. A good trade-off between computational complexity, localization and density of local minima is found by using 30×30 pixels (80% of energy in PCA).

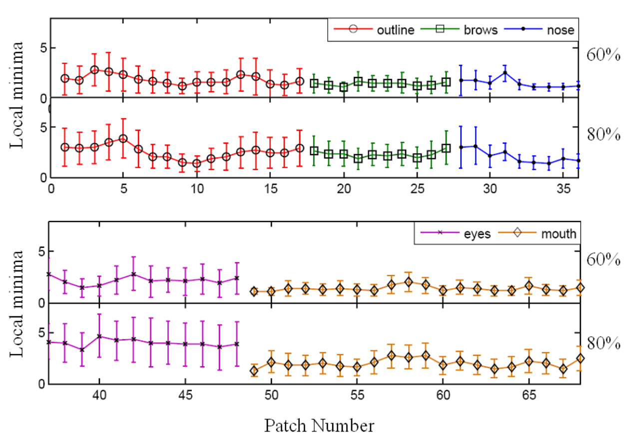

Figure 4. Mean and standard deviation of the number of local minima for each of the 68 patches. The statistics are computed for two PCA energies, 60% and 80%. See fig.(2.a).

Independently of the patch size or energy, there are some regions that generalize better than others. For instance, the patch number 34, situated below the nose, has the smallest average number of local minima. Moreover, the distance between the global minimum and the expected location of the landmark is small. In contrast, the patch number 3 situated on the left side of the outline is particularly difficult to track. It has several local minima and the distance from the global minimum to the labeled position is large. We propose to select those regions that minimize $\boldsymbol{\mu}_{patch}$:

$$\begin{aligned} \boldsymbol{\mu}_{patch} &= \boldsymbol{\mu}_{1_{patch}} + \boldsymbol{\mu}_{2_{patch}} \\ \boldsymbol{\sigma}_{patch} &= \frac{\boldsymbol{\mu}_{1_{patch}} \boldsymbol{\sigma}_{1_{patch}} + \boldsymbol{\mu}_{2_{patch}} \boldsymbol{\sigma}_{2_{patch}}}{\boldsymbol{\mu}_{1_{patch}} + \boldsymbol{\mu}_{2_{patch}}} \end{aligned} \quad (2)$$

where $\boldsymbol{\mu}_{1_{patch}}, \boldsymbol{\sigma}_{1_{patch}}$ are the mean and variance of the distance between the global minimum to the labeled one. Similarly, $\boldsymbol{\mu}_{2_{patch}}, \boldsymbol{\sigma}_{2_{patch}}$ are the mean and variance of the number of local minima. We have assumed that the distance and density of local minima are independent Gaussian random variables. Fig. (2.b) shows the best 34 patches ranked using eq. (2). The best patches are situated on the mouth, nose, eyes and some on the eyebrows.

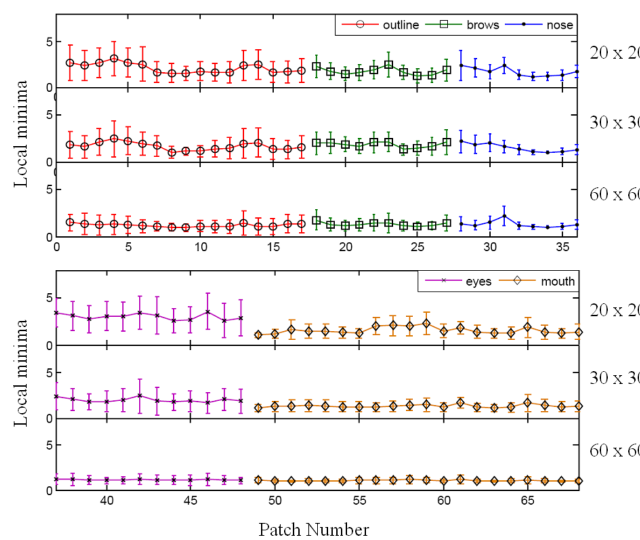

Figure 5. Mean number of local minima for each of the 68 patches. The statistics are computed for 3 patch sizes, 20×20, 30×30 and 60×60 pixels. See fig.(2.a).

4. Learning good features for ASMs

This section investigates a new methodology to build good subspace features to avoid local minima in ASMs.

4.1. Learning to model the error surface

A region with good generalization properties, ideally, would have a unique local minimum in the expected position of the landmark. A reasonable approximation would be the response of an inverted Gaussian (see fig.(6)) in a neighborhood of a particular position (x, y). Other convex non-symmetric functions are also possible.

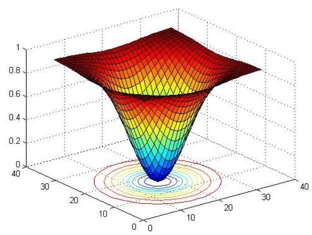

Figure 6. Inverted Gaussian response function (**R**) (32×32 pixels).

To encourage the error surface in a neighborhood to be close to an ideal one, we minimize:

$$E = \sum_{i=1}^{n} \sum_{(x,y)} (\alpha_i r_{x,y} + o_i - \frac{||\mathbf{d}_i^{(x,y)} - \boldsymbol{\mu} - \mathbf{B}\mathbf{c}_i||_2^2}{||\mathbf{d}_i^{(x,y)}||_2^2})^2 \quad (3)$$

with respect to $\mathbf{B}, \mathbf{C}$, α_i and o_i $\forall i$. $r_{x,y}$ is the desired response of the Gaussian (see fig.(6)) at the location (x, y), α_i and o_i are scale and offset factors of the ideal error surface for each image $\mathbf{d}_i$. $\mathbf{B} \in \Re^{d \times k}$ and $\mathbf{C} \in \Re^{k \times n}$ are the subspace bases and coefficients respectively. PCA is an unsupervised learning technique; however, eq. (3) is a supervised-PCA problem. Eq. (3) aims to find a subspace that has a global minimum where the landmark has been placed, and at the same time encourages the response in a certain neighborhood to be as Gaussian as possible.

At this point, it is worth pointing out three important aspects: (1) observe that we are only avoiding local minima using translational parameters. This might be seen as a limitation of the method, but it does not need to be. The optimization can handle small rotation and translation perturbations. If the ASM is used for tracking, the rotational and scale parameters can be incrementally computed after the convergence of the ASM. Normalizing the new image with the rotational and scale parameter will allow the ASM to search at a similar scale and rotation as it was previously learned. However, if the ASM is used for detection an approximate scale has to be given (e.g. from a face detector in the case of faces). (2) In our case, the inverted Gaussian has been chosen as an *ideal* error function. However, there are many other desirable convex error functions. A simple approach to have more accurate modeling of the error function will be to select for each landmark and from a set of prototypal function the one with less error. However, in our experimental validation, it has been always observed that the optimization of eq. (3) with an inverted Gaussian always improves local minima properties of the error surface. (3) Observe that if for each landmark the resulting error surface is locally convex with the global minimum in the expected place, any search algorithm (e.g. gradient descent, simplex) will succeed in fitting the ASM (assuming the shape model generalizes correctly). Observe that if few points improve their fitting properties, this will *imply* that that standard search mechanism for ASM will also improve performance.

4.2. Optimization

Our aim is to obtain a new subspace $\mathbf{B}$ able to minimize eq. (3). Unlike PCA, there is no closed form solution for the optimization of eq. (3). We alternate between solving for α_i, o_i in closed form, and performing gradient descent w.r.t. $\mathbf{B}$. These steps monotonically decrease the error of E. The gradient descent updates of $\mathbf{B}$ are given by:

$$\mathbf{B}^{n+1} = \mathbf{B}^n - \eta\mathbf{G} \qquad \mathbf{G} = \frac{\partial E}{\partial \mathbf{B}} \quad (4)$$
$$\frac{\partial E}{\partial \mathbf{B}} = \sum_{i=1}^{n} \sum_{x,y} \frac{2t_{x,y}}{||\mathbf{d}_i^{(x,y)}||_2^2} (\mathbf{d}_i^{(x,y)} - \boldsymbol{\mu} - \mathbf{B}\mathbf{c}_i^{(x,y)}) \mathbf{c}_i^{(x,y)^T}$$
$$t_{x,y} = \alpha_i r_{x,y} + o_i - f_{x,y} \qquad f_{x,y} = \frac{||\mathbf{d}_i^{(x,y)} - \boldsymbol{\mu} - \mathbf{B}\mathbf{c}_i^{(x,y)}||_2^2}{||\mathbf{d}_i^{(x,y)}||_2^2}$$

The closed form solution for α_i, o_i is given by:

$$\begin{bmatrix} \sum_{x,y} r_{x,y}^2 & \sum_{x,y} r_{x,y} \\ \sum_{x,y} r_{x,y} & \sum_{x,y} 1 \end{bmatrix} \begin{bmatrix} \alpha_i \\ o_i \end{bmatrix} = \begin{bmatrix} \sum_{x,y} f_{x,y} r_{x,y} \\ \sum_{x,y} f_{x,y} \end{bmatrix} \quad (5)$$

The major problem with the update of eq. (4) is determining the optimal η. In our case, η is found with a line search strategy [6], minimizing $E(\mathbf{B} - \eta\mathbf{G})$. It can be shown that the optimal η corresponds to the solution of the following third order polynomial:

$$a\eta^3 + b\eta^2 + c\eta + d = 0 \quad (6)$$
$$a = \sum_{i=i}^{n} \sum_{x,y} \nu^2 \qquad b = \sum_{i=i}^{n} \sum_{x,y} 3\omega\nu$$
$$c = \sum_{i=i}^{n} \sum_{x,y} 2\omega^2 - \nu t_{x,y}$$
$$d = -\sum_{i=i}^{n} \sum_{x,y} \omega t_{x,y}$$
$$\nu = \frac{\mathbf{c}_i^{(x,y)^T} \mathbf{G}^T \mathbf{G} \mathbf{c}_i^{(x,y)}}{||\mathbf{d}_i^{(x,y)}||_2^2}$$
$$\omega = \frac{\mathbf{c}_i^{(x,y)^T} \mathbf{G}^T (\mathbf{d}_i^{(x,y)} - \boldsymbol{\mu} - \mathbf{B}\mathbf{c}_i^{(x,y)})}{||\mathbf{d}_i^{(x,y)}||_2^2}$$

Experimentally, we found the roots of the polynomial always to be one real and two complex conjugate. If the three of them turn out to be real, the one that has lower error (E) value would be chosen. After each iteration, we orthonormalize the basis (i.e. $\mathbf{B}^{new} = \mathbf{B}(\mathbf{B}^T\mathbf{B})^{-0.5}$).

Minimizing eq. (3) with respect to $\mathbf{B}$ is a non-convex optimization problem prone to local minima. Without a good initial estimate of $\mathbf{B}$, the previous optimization scheme might converge to a local minimum. To get a reasonable estimation, we initialize $\mathbf{B}$ with the PCA solution. Moreover, we start from several random initial points and select the solution with minimum error after convergence.

5. Experiments

This section reports several experiments that show the benefits of our method for selecting and building better features for facial feature detection.

5.1. Selecting good regions to fit ASMs

In this experiment, we test the ability of the ASM to detect facial features in frontal faces. We compare an ASM built with 68 landmarks and an ASM built with half of the regions (34). The best regions to build an ASM are selected based on the statistics of the error surface described in section 3 using eq. (2). It is important to note that the images used to compute the statistics are not included in the training set. To ensure that the displacement error is similar in all the regions of the face, we have selected half of the patches for each region (fig. 7).

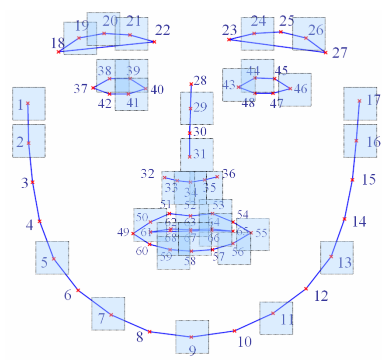

Figure 7. Best patches for each region of the face (outline, eyebrows, nose, eyes and mouth).

The algorithms are compared using 100 testing images (previously labeled). We perturb the rigid and non-rigid transformation and let the ASMs converge. Each PCA model is created using a patch of 30×30 pixels around the landmark [5]. Fig. (8) shows the perturbed and the result of the 68 lanmarks-ASM (8.a) and the 34 landmarks-ASM (8.b). The error is computed as the square difference between the labeled images and the ASM results. In this case, both ASMs converge to very similar solutions. Figure 9 shows the mean squared error (averaged over all 68 landmarks) for the 68-ASM and the 34-ASM. Using all landmarks, or the best half, does not have an impact in the detection accuracy, and it is computationally more efficient.

5.2. Learning better features to fit ASMs

This experiment shows the improvement in the statistics of the error surface to fit ASMs after learning the subspace,

a)

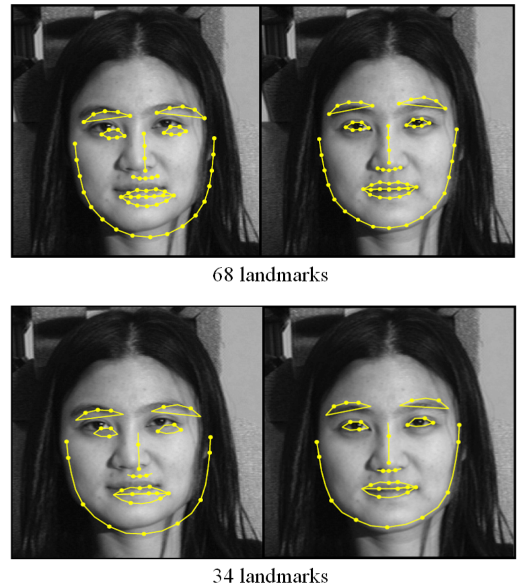

b)

Figure 8. a). ASM of 68 landmarks. Initial ASM configuration and final result. b) ASM of 34 landmarks.

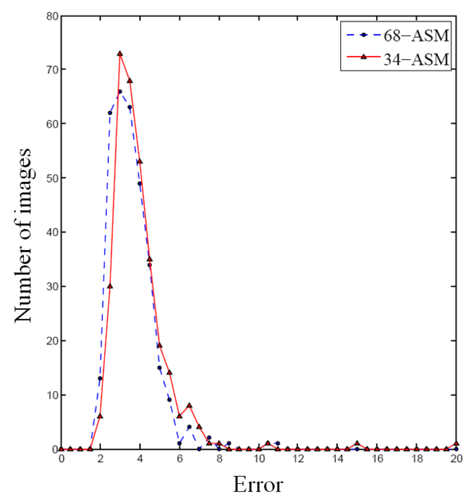

Figure 9. Error histogram using 68-ASM vs. 34-ASM.

as proposed in section 4.

The face model is learned from 200 hand-labeled images from the CMU Multi-PIE [7] database. After Procrustes is computed, we learn a subspace that optimizes eq. (3). Figure 10 shows the percentage of good patches. We consider good regions those that have a global minimum within 3×3 pixels from the labeled location of the landmark. These statistics are computed with 200 images not included in the training set. As it can be observed, our method provides a subspace that has better generalization properties for appearance tracking. An exception occurs in the nose region. In this area, the error surfaces were already good, and the algorithm spends part of the energy modeling the shape of the inverted Gaussian unnecessarily. This suggests that learning should only be applied to regions with bad local minima statistics.

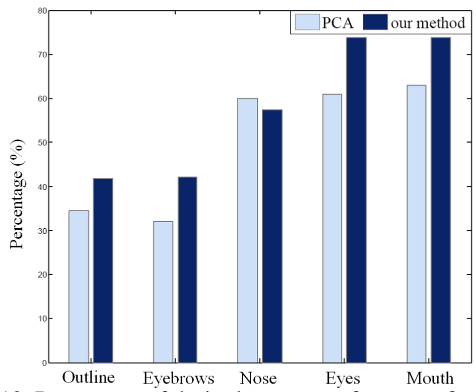

Figure 10. Percentage of desired response of error surface for two models; with and without learning good features.

Fig. (11) left shows the initial PCA-error surface for two patches. Fig. (11) right shows the results after our algorithm is applied. One patch corresponds to the eye region (40) and the other one to the mouth (63).

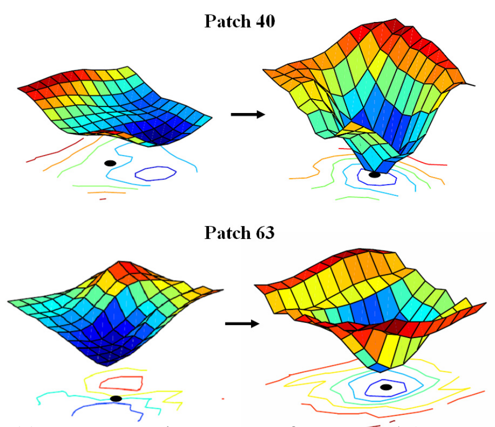

Figure 11. Reconstruction error surface around (11×11 pixels) before (left) and after (right) learning good features to track.

5.3. Detection using improved features

This section tests the ability of ASMs to fit new untrained images. As in section 5.2, a PCA model for each of the 68 landmarks is built from 200 frontal images from the Multi-pie [7] database. We use 100 testing images and randomly perturb the manual labels by a maximum of 12 pixels.

Fig. 12 shows the average error distribution for PCA and our model for 100 testing images. Both results are obtained after 2 iterations using a search window of 11×11 pixels for each landmark. As we can see, our method achieves lower error than PCA.

Acknowledgements This work has been partially supported by the U.S. Naval Research Laboratory under Contract No. N00173-07-C-2040. Any opinions, findings and conclusions or recommendations expressed in this material are those of the authors and do not necessarily reflect the views of the U.S. Naval Research Laboratory.

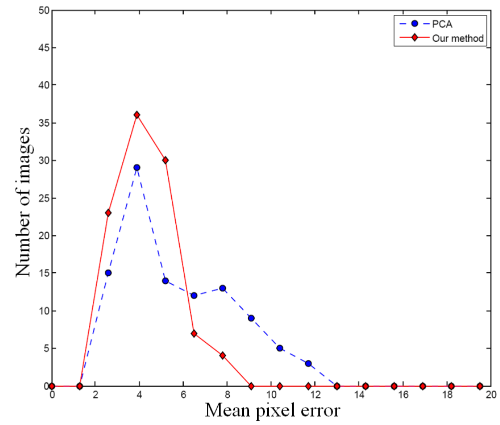

Figure 12. Error distribution using PCA and our method.

References

[1] H. Bischof, H. Wildenauer, and A. Leonardis. Illumination insensitive recognition using eigenspaces. *Computer Vision and Image Understanding*, 1(95):86 – 104, 2004.

[2] T. Cootes and C. Taylor. Statistical models of appearance for computer vision. In *Tech. Report. University of Manchester*, 2001.

[3] T. F. Cootes, C. J. Taylor, D. H. Cooper, and J. Graham. Active shape models- their training and application. *Computer Vision and Image Understanding*, 61(1):38–59, January 1995.

[4] D. Cristinacce and T. Cootes. Automatic feature localisation with constrained local models. *Journal of Pattern Recognition*, 41(10):3054–3067, 2008.

[5] F. de la Torre, A. Collet, J. Cohn, and T. Kanade. Filtered component analysis to increase robustness to local minima in appearance models. In *International Conference on Computer Vision and Pattern Recognition*, 2007.

[6] R. Fletcher. *Practical methods of optimization*. John Wiley and Sons., 1987.

[7] R. Gross, I. Matthews, J. F. Cohn, T. Kanade, and S. Baker. The cmu multi-pose, illumination, and expression (multi-pie) face database. Technical report, Carnegie Mellon University Robotics Institute.TR-07-08, 2007.

[8] M. Nguyen and F. de la Torre. Local minima free parameterized appearance models. In *International Conference on Computer Vision and Pattern Recognition*, 2008.

[9] J. Shi and C. Tomasi. Good features to track. In *IEEE Conference on Computer Vision and Pattern Recognition*, 1994.

[10] M. Wimmer, F. Stulp, S. J. Tschechne, and B. Radig. Learning robust objective functions for model fitting in image understanding applications. In *Bristish Machine Vision Conference*, 2006.

[11] H. Wu, X. Liu, and G. Doretto. Face alignment via boosted ranking model. In *Proceedings of IEEE Conference on Computer Vision and Pattern Recognition*, 2008.